Characterization of a thinned back illuminated MIMOSA V sensor as a visible light camera

Antonio Bulgheroni [a,b,*], Michele Bianda [c], Massimo Caccia [d,b], Chiara Cappellini [d], Aldo Mozzanica [d], Renzo Ramelli [c] and Fabio Risigo [a]

[a] *Università degli Studi di Milano - Milano, Italy*
[b] *Istituto Nazionale di Fisica Nucleare Sez. di Milano - Milano, Italy*
[c] *Istituto Ricerche Solari Locarno - Locarno, Switzerland*
[d] *Università dell'Insubria - Como, Italy*

Abstract

This paper reports the measurements that have been performed both in the Silicon Detector Laboratory at the University of Insubria (Como - Italy) and at the Istituto Ricerche SOlari Locarno (IRSOL) to characterize a CMOS pixel particle detector as a visible light camera. The CMOS sensor has been studied in terms of Quantum Efficiency in the visible spectrum, image blooming and reset inefficiency in saturation condition.
The main goal of these measurements is to prove that this kind of particle detector can also be used as an ultra fast, 100% fill factor visible light camera in solar physics experiments.

Key words: CMOS Imager, Spectral Response, Quantum Efficiency, Antiblooming, Image Lag
PACS: 85.60.Gz, 29.40.Gx

1. Introduction

For a long time, Charge Coupled Devices CCD have been leading the way in the field of electronics camera for all kinds of applications. Over many years, the development has been driven by an increasing market demand for larger and larger pixel numbers and better image quality that no other technology could provide. However, interest in image sensors based on standard Complementary Metal Oxide Semiconductor (CMOS) technology has grown significantly in the past years. CMOS based imagers offer significant advantages over CCDs such as system-on-chip capability, standard commercially available technology, low power consumption and possibly lower cost [1, 2]. Moreover the possibility to readout only a reduced number of sparsified pixels in the matrix makes CMOS imager an appealing CCD competitor especially in fast applications.
In the early days of the CMOS imager story, one of the main disadvantages was the limited fill factor [1] due to the aluminum tracks connecting each

* Corresponding author.
Email address: antonio.bulgheroni@mi.infn.it (Antonio Bulgheroni).

[1] This is defined as the ratio between the sensitive surface and the total sensor area.

pixel to the readout electronics and to the peripheral addressing circuitry. Furthermore, since in a CMOS imager the sensitive volume is a few hundreds of micrometers deep from the wafer backplane, back illumination with visible photons was hardly achievable.
Since the fill factor is not an issue in high energy elementary particle tracking and imaging, physicists adopted CMOS imagers, suitably modified to fulfill their requirements, as an attractive alternative solution to hybrid pixel detectors and to CCD [3] in future High Energy Physics (HEP) experiments.
In HEP experiments, the main role of this kind of sensors is the identification of a particle track through the determination of its collision point on several sensor layers [4]. To reduce multiple scattering, the total thickness of passive and active material has to be kept as low as possible. Moreover, removing insensitive layers increases the sensitivity to short range particle. For this purpose a major development in the CMOS imager technology to remove the passive layer from the backplane has been recently carried out by the SUCIMA [2] consortium [6, 7, 8]. Due to the back thinning development, back illumination visible light detection is now achievable with a 100% filling factor and the CMOS imager potential can be fully exploited. Because of a non disclosure agreement signed between the SUCIMA consortium and an industrial partner, technological details about the back thinning process cannot be revealed.
This paper describes the tests performed both at the Silicon Laboratory at the University of Insubria in Como and at the Istituto Ricerche SOlari Locarno (IRSOL) in order to characterize a thinned CMOS imager for visible light detection. The characterization experiments were aimed to estimate the sensor Quantum Efficiency (QE) in the visible part of the electromagnetic spectrum, the image blooming and time latency in over saturation conditions.

[2] Silicon Ultrafast Camera for electron and γ sources in medical applications (SUCIMA) is a completed project approved in the Fifth Framework Program by the European Commission under the Contract G1RD-CT-2001-00561 [5]

2. The MIMOSA CMOS imager

The CMOS imager being characterized in these experiments belongs to a family of sensor called Minimim Ionising MOS Active pixel sensor (MIMOSA) whose development was pioneered and still is driven by the LEPSI/IReS teams in Strasbourg [9]. A picture of the device under test is shown in Figure 1 and its main characteristics are reported in Table 1.

Table 1
MIMOSA 5 main characteristics

Size	1020 × 1024 pixels
Pixel pitch	$17 \times 17\,\mu m^2$
Readout frequency	> 40 MHz
Parallel analog output	4 channels
Frame readout time (@ 10 MHz)	26 ms
Technological process	$0.6\,\mu$m AMS
Epitaxial (sensitive) layer	$\approx 14\,\mu$m
Conversion gain	7.3 ADC/e^-
CCE after thinning	50% - 60%
Camera gain	10.6 ADC/e^-

Fig. 1. *A MIMOSA 5 sensor glued on a PCB adapter board.*

The sensor has been tested with high energy particles to study the detection and the charge collection efficiency, the spatial resolution and the charge to voltage conversion gain for different layout geometries.
Within the SUCIMA project, a major effort has

been invested to push an extreme backthinning down to the epitaxial layer with an entrance window of $\sim$ 100 nm. Tests using dedicated setups have shown that the thinned sensor sensitivity to short range particles is clearly enhanced and among all the detector performances only the Charge Collection Efficiency (CCE) is reduced at the 50% - 60% level after the post-processing [6].

3. Quantum Efficiency measurement

One of the most important feature of a visible light detector is its QE representing the number of charge carriers produced by one impinging photon. The region of interest of the electromagnetic spectrum, corresponding to the visible part and the near infra-read, is from 400 to 850 nm thus the sensor QE dependence on wavelength should be as flat as possible in that range and high enough to assure an acceptable sensitivity level. From a theoretical point of view [10], the QE wavelength dependency should reach a maximum when the corresponding photon energy is close to the forbidden energy gap. The output signal S measured in ADC units of a single sensitive element exposed to a monochromatic photon may be written as follows:

$$S = \Phi_\lambda \, \eta_\lambda \, g \, \Delta t \, A \tag{1}$$

where:
- Φ_λ is the photon flux for a given wavelength λ measured in photons per second per unit of area;
- η_λ is the QE at a given wavelength λ measured in charge carriers per photon;
- g is the sensor and amplification system overall conversion gain in ADC units per charge carrier;
- Δt is the exposure time;
- A is the surface of the sensitive element.

Using this formula the QE of a sensor under investigation can be measured referring its signal to a detector with known QE exposed to the same flux.

3.1. *Experimental setup*

Following the approach described in the previous section, the QE of the MIMOSA 5 sensor has been studied comparing the output signal of both the CMOS and the Wright AT1 CCD camera available at IRSOL. The spectral response and the main features of the reference camera were made available by the producer [3]. Taking advantage of the use of the IRSOL spectrograph, six narrow spectral intervals of the solar light were recorded using the two cameras at 400, 500, 630, 701, 760 and 850 nm. Each spectral window has been chosen in a way to have at least two absorption lines in the image in order to define the linear function $\Lambda(x)$ to translate the pixel position on the MIMOSA sensor in the corresponding wavelength value according to the following equation (2)

$$\Lambda(x) = \left(\frac{y_1 - y_2}{x_1 - x_2} \right) x + \left(\frac{y_2 x_1 - y_1 x_2}{x_1 - x_2} \right) \tag{2}$$

where:

$$x_i \xrightarrow{\Lambda} y_i$$

are the two reference points.
Particular care has been spent to keep the experimental conditions in the two measuring setups as close as possible. For this purpose during the data acquisition the solar light intensity was monitored and only variations at the few percent level were recorded. Due to the readout scheme [11], the MIMOSA 5 exposure time was kept constant for all the spectral images while the CCD integration time was properly adjusted to best fit the dynamic range. To make the output of the two cameras comparable, a normalization factor has been introduced to take into account the different exposure time, the sensitive cell area and the overall conversion gain. The last one is well known for the CCD camera, while for the MIMOSA the value obtained with the ^{55}Fe calibration (Table 1) was used and the reduced charge collection efficiency taken into account.

3.2. *Data analysis*

For each spectral region, 200 frames have been acquired, background subtracted and averaged to reduce the noise fluctuations. The two dimensional images have been projected along the spectral axis that has been calibrated using two absorption lines

[3] `http://www.e2v.com/datasheets/charge_coupled_devices_ccds/ccd62-06ims.pdf`.

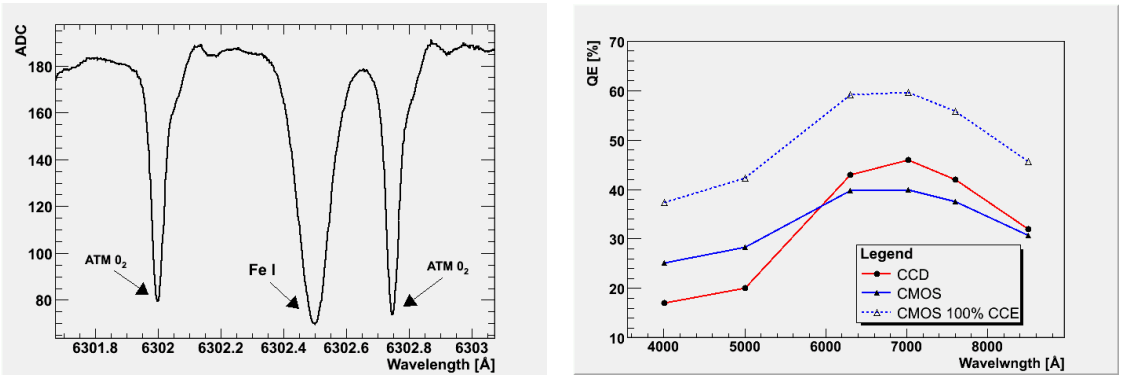

(a) ***Spectrum at 630 nm***

(b) ***QE comparison***

Fig. 2. *Spectral response of the MIMOSA sensor compared with the reference CCD. The dashed line represents the QE achievable with a 100% CCE.*

and comparing their positions with the one reported on the National Solar Observatory solar atlas [4] . The obtained spectrum has been compared with the one acquired with the reference front illuminated CCD. From the CCD measurements, the value of the solar photon flux for each spectral window has been estimated and used to calculate the QE of the MIMOSA 5 sensor. The obtained results are shown in Figure 2.
As expected, the MIMOSA 5 sensor, being a back illuminated device, has a better QE than CCD in the ultraviolet region while the thin sensitive layer is reducing the sensibility to infrared radiation. The benefit arising from the thinning and the back illumination, i. e. the 100% fill factor, are somehow spoiled by the reduced CCE [7]. Technologists are now considering some solutions to restore the almost complete CCE after the backthinning, this will result in a net improvement of the QE as shown by the dashed line in Figure 2, making the use of this kind of sensor even more appealing.

[4] Courtesy of NSO/Kitt Peak. The Fourier Transform Spectrometer data used here were produced by NSF/NOAO.

4. Image blooming

In many experimental conditions, having images with regions particularly intense and other almost completely dark is not uncommon. This is true, for instance, when dealing with spectral images in which almost pure black absorption lines should be compared with a bright continuum. In these cases, setting a proper exposure time is an issue because on one hand, it can not be too short in order to have enough statistics in the dark region and, on the other hand, it can not be too long to avoid saturation in the bright one. Moreover in saturation condition, the brightest part of the image tends to grow in size (*blooming*) and in the worst case it can occupy the full sensitive surface of the sensor.
The physical explanation of the image blooming effect in saturation condition can be related to the charge carrier diffusion and in the case of CCDs to the charge transfer mechanism. In CCD cameras, this is a well known problem and several anti-blooming techniques have been implemented the *anti-blooming gate* being the more common. Anti-blooming gates built into the CCD occupy about 30% of the pixel area. The result is a reduced fill factor and sensitivity. Furthermore, the area of the CCD occupied by the anti-blooming gate leaves a significant gap between pixels, reducing the effective resolution of the sensor.

CMOS sensors should be naturally immune from blooming since each pixel is directly connected to the readout line switching on two selection transistors [2]. But, if the injected charge density in a region of the sensor is too high, charge carrier diffusion and electronic cross-talk may result in an image deformation and enlargement.

4.1. *Experimental setup*

A dedicated measuring setup has been assembled to characterize the MIMOSA image blooming when exposed to an over-saturating flux of visible light photons.
The setup consists of a He-Ne laser ($\lambda = 633$ nm) source with a maximum emitted power of 10 mW. The laser light passes through a polarizer - analyzer pair to have a variable light intensity. Due to the Gaussian shaped intensity profile of the emitted light, only a small central region of the laser profile has been selected using a 1 mm diameter pin-hole to decrease the intensity inhomogeneity. The pin-hole has been kept as close as possible to the MIMOSA sensor in order to reduce the beam divergence. Moreover to further reduce the laser intensity a spectral filter can be inserted in the light path in between the analyzer and the pin-hole.
An absolute measurement of the light intensity arriving on the sensor surface is not trivial; to estimate it with a reasonable accuracy a part of the laser light has been collected by a photodiode. The intensity measured by the photodiode is proportional to the one arriving on the MIMOSA.

4.2. *Data analysis*

Twenty images of the pin-hole corresponding to 10 different polarizer-analyzer angles with and without the spectral filter have been acquired and analyzed. The light intensity measured by the photodiode has been varied over 8 orders of magnitude: with the first 4 decades obtained with the spectral filter on the light path. The pin-hole image is an ellipse with an almost unitary degree of eccentricity [5]. The increased size of the hole image can be demonstrated considering the length of the two radii as a function of the light intensity as shown in Figures 3.
The hole image size has been measured to be statistically constant over the first four orders of magnitude while an increase of ~ 1.5 times in the radius length occurred over the last four decades. The radius length increase started with the sensor saturation. It should be underlined that, since the sensor was designed for high energy particle tracking, its dynamic range is very limited and not optimized for visible light applications.

5. Image lag

All sensitive devices are characterized by a certain dead time during which they are not ready to detect a new physical information because either they are being read out or they are being reset to the initial condition. For sensors like visible light cameras, another common fault is the image latency, usually related to a non completely efficient reset mechanism. Also human retina, for instance, is affected by the same effect, and when someone looks a very intense light source, even after she/he closes her/his eyes, the image stays there clearly visible for a certain period of time.
In a CMOS camera there are two different phenomena possibly leading to an image latency after the pixel contents are cleared:

Charge collection time constant. CMOS sensors are almost completely undepleted devices and in the sensitive volume no external drifting potential is applied. As a consequence, the charge collection can occur only because of diffusion and the collection time is at least one order of magnitude greater than the typical values obtained in drift-based sensors. The charge collection can be thought as a mechanism with a

[5] The pin-hole has been fabricated by drilling a hole in a squared 2 cm edge aluminum plate. To avoid light reflection, a black adhesive tape has been glued on both sides of the plate. To make the hole also in the tape the tip of a hot needle has been used and this could have been the origin of the image eccentricity.

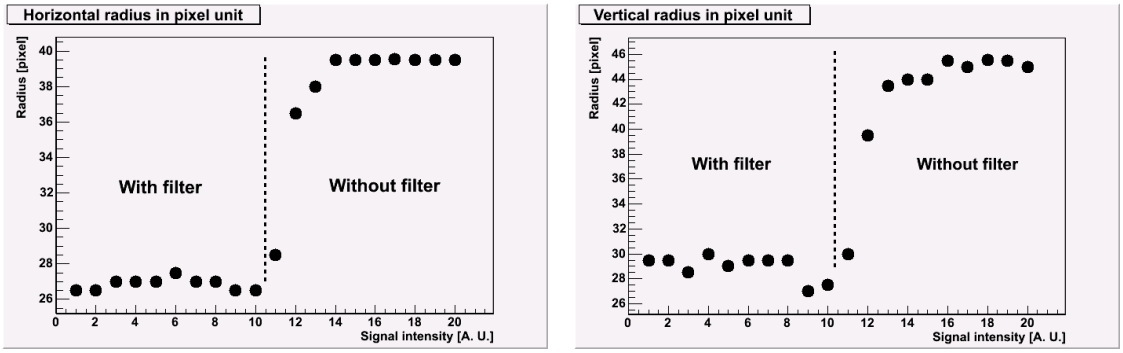

(a) ***x radius*** **(b)** ***y radius***

Fig. 3. *Length of the detected hole image diameters as a function of the light intensity. The light intensity has been spanned over 8 orders of magnitude. In the two flat regions, fluctuations in the radius lenght of one or two pixels are not significant.*

certain time constant and its time dependence is such that not all of the generated charge is collected during an integration time, and a charge leftover can be collected by the pixel afterward. Moreover, charge carriers might be blocked into traps and released with a longer time constant.

Reset inefficiency. Every readout cycle each photodiode is directly connected to the bias line via the reset transistor in order to clear the pixel content [11]. Depending on the applications, the user can decide how often the pixel should be reset [6] and how long the photodiode should stay connected to the bias line.

Especially when the sensor is exposed to a large flux of photons, the duration of the reset is not changing very much the reset efficiency [12] but overdriving the reset transistor will reduce the image lag at the expense of a higher reset noise. Overdriving means forcing the reset transistor to work in its linear region for the whole duration of the reset period. In this way, the photodiode voltage after the reset is independent from its initial value. This so called *hard reset* can be obtained connecting the reset transistor gate not to the same bias line used for the other transistors, but to a lower voltage ($\sim 2/3 V_{dd}$). This is possible with the MIMOSA sensor, because the bias line for the reset transistor is kept separated from the other ones. The main drawback of the *hard reset* is a reduced dynamic range and an increased reset noise.

[6] This feature is of particular interest in HEP experiments, where the number of hit pixels per event is very limited.

5.1. *Experimental setup*

To measure the image lag due to incomplete reset, a setup similar to the previous one has been used in which a triggerable mechanical shutter has been placed into the laser path. The shutter and its controller provide accurate and repeatable exposures as short as 9.2 ms with a maximum frequency of 200 Hz. The shutter controller can be steered by the Data Acquisition system (DAQ) via a TTL signal defining the shutter opening and the exposure duration. Using the shutter, the continuous He-Ne laser has been pulsed on the sensor surface with a precise timing. Using the standard Correlated Double Sampling (CDS) algorithm, no image lag has been detected. This is something one can imagine due to the CDS reduced reset noise [12]. A faint image lag was, instead, measured when the CDS method was not applied and only the last of the two following frames considered. To be able to distinguish from the real image produced by the laser and its shadow due to the image lag, the laser was shone on the sensor according to the timing described below and sketched in Figure 4.

The acquisition cycle was made by four frames and a continuous point-like laser spot was shone on the

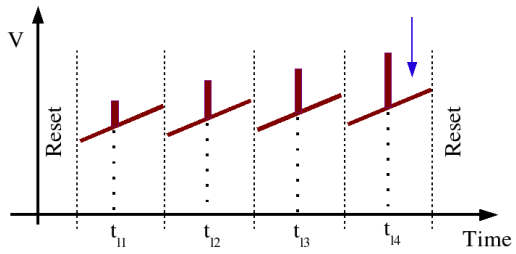

Fig. 4. *Schematic diagram of the sensor analog output when a continuous point-like laser spot is shone on the sensor. This allows to determine the position – time correspondence set by the MIMOSA readout scheme. The t_{l_n} represent the positions of the laser spot on the four acquired frames. The arrow indicates the instant in which the laser was shot in the image lag experiment.*

sensor in a precise and fixed spatial position. The sensor analog output, as can be observed on the scope, will present the typical sawtooth shape with regularly spaced bunches of pixels with higher signal corresponding to the laser as detected in the four frames. In this way t_{l_n}, one per frame, can be defined as the temporal correspondence of the spatial position. For instance, t_{l_1} represents the instant when the pixels on which the laser is shone are readout, or in other words, for how long those pixels integrated the laser induced charge during the first frame. This also explains why the laser signal is increasing going from the first to the last frame.

Let us consider now the case in which the laser is pulsed and a short pulse is shot on the sensor in between t_{l_1} and t_{l_2}: one is bound not to see any signal on the first frame, while a constant signal appears in the last three. If the laser is shone on the sensor with a delay such to arrive after t_{l_4} and before the readout cycle end (the arrow in Figure 4) the analog output should appear *empty* because the charge integration is occurring after the last readout. In fact, if the reset mechanism is not 100% efficient a faint image may appear in the next first frame after the reset.

The reset transistor overdriving has been obtained connecting the reset transistor gate line to an external tunable power supply V_{ddr}.

5.2. *Data analysis*

Using the time structure described above, 200 frames in which a laser spot has been shone in between t_{l_4} and the next reset have been taken with the standard reset circuit and with the *hard reset* implemented. The polarizer – analyzer pair has been tuned in order to have a medium intensity light passing through the pin hole and arriving on the sensor. The obtained images, averaged over the 200 acquired frames, have been sliced horizontally and shown in Figure 5. In the case of the standard reset circuit, a left-over signal, representing roughly the 10% of the injected charge, is found, while it is completly removed using the hard reset technique.

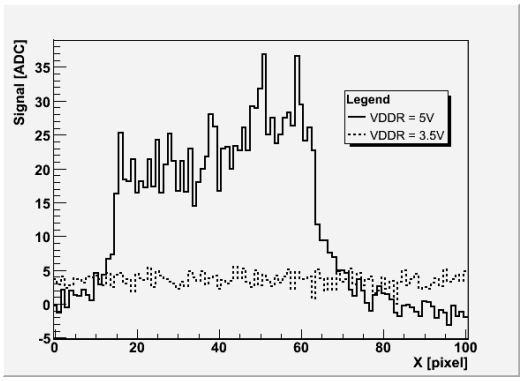

Fig. 5. *Horizontal slice of the image lag with and without the hard reset.*

The use of the hard reset technique presented two major drawbacks: a reduction in the dynamic range and the presence of unexpected baseline shift as shown in Figure 5 the orign of it is still under investigation.

6. Conclusion

A CMOS imager called MIMOSA designed for high energy particle tracking and imaging has been characterized as a visible light sensor for application in spectrographic experiments. The QE of the MIMOSA sensor in the visible range of the spectrum has been measured for the first time ever and performance comparable to the one of

a scientific grade CCD camera has been obtained with an even more flat behavior. The sensitivity in the near UV range is enhanced even without any particular coating. The benefit arising from the thinning and the back illumination are somehow spoiled by the reduced CCE. The possibility to restore the CCE after the thinning post process is under investigation and may result in a superior spectral response.

The sensor demonstrated itself to be blooming immune at least for a light intensity scan covering four order of magnitude. For saturating and over saturating photon fluxes a maximum increase of 1.5 times of the image radius has been observed.

The image latency on the electronics retina has been measured using a suitable laser timing. No image lag has been detected when the sensor was operated in the standard CDS mode. The effectiveness of the *hard reset* technique, i. e. forcing the reset transistor to operate in the linear regime during the whole reset time has been demonstrated to completely remove the faint image lag when the CDS processing was not performed. As a consequence of the hard reset, a dynamic range reduction at the 25% level has been measured along with an unexpected baseline shift. A suitable trade off between reset efficiency and dynamic range must be found depending on the application specific requirements.

Acknowledgements

The authors would like to thank all the SUCIMA consortium partners. Special thanks to W. Dulinski from IReS/CNRS (Strasbourg) and G. Deptuch currently with Brookhaven National Laboratory for the help provided in understanding the working principle of the MIMOSA sensor and to A. Czermak and B. Dulny from the Institute of Nuclear Physics in Krakow for the precious collaboration in the development of the DAQ system.

References

[1] E. R. Fossum, CMOS image sensors: electronic camera-on-a-chip, IEEE Transactions on Electronics Devices 44 (10) (1997) 1689.

[2] D. Litwiller, CCD vs. CMOS: Facts and Fiction, Photonics Spectra.

[3] R. Bailey, C. J. S. Damerell, First measurements of efficiency and precision of CCD detectors for High Energy Physics, Nucl. Instrum. Meth. A 213 (1983) 201–215.

[4] R. Turchetta, J. D. Brest, B. Casadei, G. Claus, C. Colledani, W. Dulinski, Y. Hu, D. Husson, J. P. Le Normand, J. L. Riester, G. Deptuch, U. Goerlach, S. Higueret, M. Winter, A monolithic active pixel sensor for charged particle tracking and imaging using standard VLSI CMOS technology, Nucl. Instrum. Meth. A 458 (2001) 677–689.

[5] M. Caccia, et al., Silicon ultra fast cameras for electron and γ sources in medical applications, Nucl. Phys. B (Proc. Suppl.) 125 (2003) 133–138.

[6] W. Dulinski, A. Braem, M. Caccia, G. Claus, G. Deptuch, D. Grandjean, C. Joram, J. Séguinot, M. Winter, Tests of a backside illuminated monolithic CMOS pixel sensor in an HPD set-up, Nucl. Instrum. Meth. A 546 (2005) 274 – 280.

[7] G. Deptuch, Tritium autoradiography with thinned and back-side illuminated monolithic active pixel sensor device, Nucl. Instrum. Meth. A 543 (2005) 537 – 548.

[8] G. Deptuch, W. Dulinski, M. Caccia, M. Winter, High resolution back-side illuminated monolithic active pixel sensors for low energy electron imaging, IEEE Trans. Nucl. Sci. 52 (2005) 1745 – 1754.

[9] G. Claus, et al., Particle tracking using CMOS monolithic active pixel sensor, Nucl. Instrum. Meth. A 465 (2000) 120–124.

[10] E. Antončík, N. K. S. Gaur, Theory of the quantum efficiency in silicon and germanium, J. Phys. C: Solid State Phys. 11 (1978) 735–743.

[11] G. Deptuch, New generation of monolithic ac-

tive pixel sensors for charged particle detection, Ph.D. thesis, École Doctorale Physique, Chimie physique et Matèmatiques - Université Luis Pasteur, Strasbourg - France (2002).
[12] H. Tian, B. Fowler, A. El Gamal, Analysis of Temporal Noise in CMOS Photodiode Active Pixel Sensor, IEEE J. of Solid-state circuits 36 (1) (2001) 92–101.